# Second Harmonic Generation from an NLO Dye Aligned by the Internal Electric Field in a Blend of Poly(vinylidene fluoride) and Poly(methyl methacrylate)

**Naoto Tsutsumi,* Ichiro Fujii, Yoshiaki Ueda, and Tsuyoshi Kiyotsukuri**

*Department of Polymer Science & Engineering, Kyoto Institute of Technology, Matsugasaki, Sakyoku, Kyoto 606, Japan*

*Received March 18, 1994; Revised Manuscript Received December 1, 1994®*

ABSTRACT: This paper presents a measurement of the second harmonic generation (SHG) from the nonlinear optical (NLO) dyes oriented by the internal electric field ($E_i$) created by the preferential alignment of $\beta$-crystallite dipoles in a poled blend of 80 wt % poly(vinylidene fluoride) and 20 wt % poly(methyl methacrylate) with optical clarity. SHG coefficients $d_{33}$ and $d_{31}$ are investigated as a function of NLO dye concentration and compared to the theoretical values. The thermal stability of $d_{33}$ and $d_{31}$ is studied, which has been compared those of $E_i$ and the pyroelectric coefficient reported in a previous paper.[10]

## Introduction

Extensive studies have been made on fabricating thermally stable nonlinear optical (NLO) polymeric materials.[1−7] One approach is the use of cross-linking to suppress the segmental molecular motion of the polymer matrix.[2,4−6] Another approach is the utilization of a high glass transition temperature ($T_g$) material, such as polyimide, for the thermally stable host in a guest−host NLO system.[7]

Tsutsumi et al.[8] have studied the internal electric field ($E_i$) created by the aligned $\beta$-crystallite dipoles of the copolymer of vinylidene fluoride and trifluoroethylene (P(VDF−TrFE)) using the electrochromic spectrum shift of a dye dissolved in the copolymer, and discussed the correlation between $E_i$ and remanent polarization as well as the thermal stability of $E_i$. Tsutsumi et al. have also measured the internal electric field in the blend of 80 wt % poly(vinylidene fluoride) (PVDF) and 20 wt % poly(methyl methacrylate) (PMMA) prepared by melt-quenching and successive annealing[9,10] and that in the blends of P(VDF−TrFE) and PMMA,[11] using the same procedure as in the case of P(VDF−TrFE).[8] When these ferroelectric hosts are well-poled, they have the internal electric field in the range $2 \times 10^6$−$4 \times 10^6$ V/cm, which is approximately 3 or 4 times larger than the poling field. When dye molecules, which have NLO properties, are dispersed in these matrices, this strong internal electric field stabilizes the alignment of NLO molecules. Furthermore, ultraviolet−visible spectroscopic measurement showed that the blend of 80/20 wt % PVDF/PMMA remains clear and transparent in the wavelength range from 350 to 750 nm even after the annealing treatment.[10] Thus, because ferroelectric polarization can be induced in such a blend, it appears to be a promising host material in a guest−host NLO system where the guest is an optically nonlinear dye molecule that is orientationally stabilized by the strong internal electric field of the poled ferroelectric.

Recently, we have measured that the second harmonic generation (SHG) in the blend of PVDF/PMMA can be increased by the incorporation of NLO dyes in the matrix, which have been preferentially aligned by the internal electric field created by the oriented polar PVDF crystallite dipoles and found that the thermal stability of SHG corresponds well to the thermal stability of the oriented polar PVDF crystallite dipoles. In this paper, we report SHG from the NLO dyes aligned by the internal electric field created by the oriented polar PVDF crystallite dipoles and investigate the dependence of SHG on the NLO dye concentration and the thermal stability of SHG.

## Experimental Section

**Sample Preparation.** PVDF (Kureha KF-polymer, $M_w$ = 141 000, $M_n$ = 64 000) and PMMA (Mitsubishi Rayon Acrypett-VHK, $M_w$ = 168 000, $M_n$ = 96 400) were used. The NLO dyes of 4-(dimethylamino)-4′-nitrostilbene (DANS) from Eastman Kodak Co. and 4-(dimethylamino)-4′-nitroazobenzene (DANAB) from Tokyo Kasei Co. were used. DANS is also an electrochromic probe for internal electric field calculation. DANS was recrystallized from amyl alcohol solution. DANAB was used as received. A DMAc solution of the blend polymer of PVDF/PMMA (80/20 by weight) with an NLO dye of a given concentration was cast to obtain films. After drying the cast films, they were melt-pressed between 50 $\mu$m thick films of Upilex (Ube Industry) on a heated press to a thickness between 30 and 40 $\mu$m. Then the molten films were quenched into liquid nitrogen and annealed at 120 °C for 2 h before poling. The blend films were poled by applying a constant field of 0.7 MV/cm for 1 h at 80 °C in a nitrogen atmosphere or in Fluorinert to aluminum electrodes which had been evaporated onto opposing surfaces of the films.

**Electrical and Optical Measurements.** After the samples were poled, the aluminum electrodes were removed by immersing in 0.1 N NaOH for a few minutes in order to make the subsequent optical measurements. Ultraviolet−visible spectra of the samples were measured on a Shimadzu model UV-2101PC spectrophotometer controlled by a PC microcomputer. The measured spectra were obtained in transmission and were stored by 0.5 nm intervals in a microcomputer for analysis.

Refractive indices (RI) of the films were measured using a Atago Abbe refractometer model 1T with monochromated light through an interference filter at 470, 530, 610, 660, and 1060 nm. When RI was measured at 1060 nm, a near infrared viewer was used to convert near infrared light to visual.

The SHG was measured by the Maker fringe method.[12,13] The laser source was a Continuum model Surelite-10 Q-switched Nd:YAG pulse laser with a 1064 nm $p$-polarized fundamental beam (320 mJ maximum energy, 7 ns pulse width, and 10 Hz repeating rate). The generated second harmonic (SH) wave was detected by a Hamamatsu model R928 photomultiplier. The SH signal averaged on a Stanford

* To whom all correspondence should be addressed.

® Abstract published in *Advance ACS Abstracts,* January 15, 1995.

0024-9297/95/2228-0950$09.00/0 

Research Systems (SRS) model SR-250 gated integrator and boxcar averager module was transferred to a microcomputer through an SRS model SR-245 computer interface module. The detailed experimental procedure is described in ref 11.

**Characterization.** Wide angle X-ray scattering (WAXS) patterns of the films were measured with a Toshiba model ADG-301 X-ray diffractometer with nickel-filtered Cu Kα radiation, and the obtained patterns were transferred to a microcomputer for data analysis. Differential thermal analysis (DTA) was carried out using a Shimadzu model DT-30 differential thermal analyzer at a heating rate of 10 °C/min in nitrogen atmosphere.

**Basis for Measurement of the Internal Electric Field.** A theory for electrochromic effects in liquid solutions was developed and published by Liptay and co-workers in a series of papers which are well summarized in a book chapter.[14] The theory was applied to electrochromic molecules dissolved in a polymer matrix by Havinga and van Pelt.[15] Stated simply, optical absorption corresponds to energy transfer between an electronic ground and an electronic excited state in a molecule. In the presence of an electric field, the energy of each state is reduced by the product of the dipole moment $\mu$, the field $E$, and the cosine of the angle between the dipole and the field. The energy difference between the ground and the excited states at a particular angular position is then altered by an amount proportional to the electric field and the difference in dipole moment between the two states. The angular distribution of dipoles with respect to the field is estimated from the Langevin function in terms of the dimensionless variable $\mu E/(kT)$. Molecular parameters which enter the theory are the dipole moments of the ground state $\mu_g$ and the excited state $\mu_e$ and the angles between the dipole moments and a coordinate system within the molecule. For large values of $\mu$, terms involving the polarizations of the two states are negligible.

The absorption spectra of the probe molecules are rather broad and the shifts in the peak maxima are small so that spectra shifts are best determined by comparing large proportions of the two spectra. For this purpose, it has been found convenient to express the spectrum in the presence of a field $A(\nu,E)$ as a Taylor series expansion of the unperturbed spectrum $A(\nu,0)$ with the wavenumber shift $\Delta\nu$ as the perturbation. Furthermore, according to Liptay[14] the absorption spectrum is practically identical to a Lorentzian line shape if expressed as absorbance divided by wavenumber. Following Havinga and van Pelt,[15]

$$\frac{A(\nu,E)}{\nu} - \frac{A(\nu,0)}{\nu} = \delta\frac{A(\nu,0)}{\nu} + \langle\Delta\nu\rangle\frac{\partial}{\partial\nu}\frac{A(\nu,0)}{\nu} + \frac{1}{2}\langle(\Delta\nu)^2\rangle\frac{\partial^2}{\partial\nu^2}\frac{A(\nu,0)}{\nu} \quad (1)$$

The term involving $\delta$ accounts for a change in absorbance due to reorientation of the dye in the presence of the field. Terms involving $\langle\Delta\nu\rangle$ and $\langle(\Delta\nu)^2\rangle$ describe field-induced shifts in the band and field-induced broadening of the band,[19] respectively. The decrease of absorption intensity by poling is due to not only the reorientation (alignment) of DANS to the internal field but also the loss of some DANS when the sample is poled at 80 °C and annealed at high temperature up to 130 °C. If we assume that the intensity of the absorbance is reduced uniformly by a factor $f$ across all wavelengths in the absorption band and neglect terms above $\langle(\Delta\nu)^2\rangle$, the poled spectrum can be expressed in terms of the unpoled spectrum by

$$\frac{1}{(1-f)}\frac{A(\nu,E)}{\nu} - \frac{A(\nu,0)}{\nu} = \delta\frac{A(\nu,0)}{\nu} + \langle\Delta\nu\rangle\frac{\partial}{\partial\nu}\frac{A(\nu,0)}{\nu} + \frac{1}{2}\langle(\Delta\nu)^2\rangle\frac{\partial^2}{\partial\nu^2}\frac{A(\nu,0)}{\nu} \quad (2)$$

The theoretical expressions for $\delta$, $\langle\Delta\nu\rangle$, and $\langle(\Delta\nu)^2\rangle$ in the paper of Havinga and van Pelt[15] can be modified[8] to simplified forms of

$$\delta = -G(u) \quad (3)$$

$$\langle\Delta\nu\rangle = -\frac{G(u)}{1-G(u)}3C \quad (4)$$

$$\langle(\Delta\nu)^2\rangle = \frac{G(u)}{1-G(u)}3C^2 \quad (5)$$

$$G(u) = 1 - \frac{3\coth(u)}{u} + \frac{3}{u^2} \quad (6)$$

$$u = \frac{E_i\mu_g}{kT} \quad (7)$$

$$C = \frac{kT\Delta\mu}{hc\mu_g} \quad (8)$$

where $k$ is Boltzmann's constant, $T$ is the absolute temperature, $\Delta\mu$ is the difference between the dipole moments in the excited state and in the ground state ($=\mu_g - \mu_e$), $h$ is Planck's constant, and $c$ is the speed of light. Substitution of the expressions for $\delta$, $\langle\Delta\nu\rangle$, and $\langle(\Delta\nu)^2\rangle$ in eq 2 by eqs 3–5, respectively, and the subsequent rearranging results in the final equation of

$$\frac{1}{(1-f)(1-G(u))}\frac{A(\nu,E)}{\nu} - \frac{A(\nu,0)}{\nu} = \frac{G(u)}{(1-G(u))^2}\left[-3C\frac{\partial}{\partial\nu}\frac{A(\nu,0)}{\nu} + \frac{3}{2}C^2\frac{\partial^2}{\partial\nu^2}\frac{A(\nu,0)}{\nu}\right] \quad (9)$$

**Calculation of the Internal Electric Field.** The difference in the absorbances divided by $\nu$ at several values of $\nu$ between before and after poling would be fit to the original spectrum and the first and second derivatives of the original curves at the corresponding wavenumbers according to eq 1. Coefficients obtained from such a fit are the orientation-induced change in absorbance $\delta$, the shift in absorption spectra $\langle\Delta\nu\rangle$, and the broadening of the peak $\langle(\Delta\nu)^2\rangle$. However, as mentioned above, changes in absorbances are also caused by a decrease in the concentration of dye. We have introduced the theoretical expression by including factor $f$ of eq 2 and arrived at eq 9 involving the electric field, dipole moment, etc., of eqs 3–5.

The spectrum after poling, reduced from the original by factors $f$ and $G(u)$, shifted by $\Delta\nu$ and broadened by $\langle(\Delta\nu)^2\rangle/2$, will cross the original spectrum at some value of wavenumber $\nu_N$, where $A(\nu_N,E)/[(1-f)\{1-G(u)\}\nu_N] = A(\nu_N,0)/\nu_N$. At the intersection, the right-hand side of eq 9 will be equal to zero, from which it can be deduced that $\partial\{A(\nu,0)/\nu\}/\partial\nu = (C/2)\partial^2\{A(\nu,0)/\nu\}/\partial\nu^2$. First and second derivatives of $A(\nu,0)/\nu$ are evaluated as a function of $\nu$ to determine the value $\nu_N$ for which the above relation was satisfied. A value of $(1-f)\{1-G(u)\}$ was then chosen to make the spectra of the poled and unpoled samples intersect at $\nu_N$, i.e. $A(\nu_N,E)/[(1-f)\{1-G(u)\}\nu_N] = A(\nu_N,0)/\nu_N$. Having normalized the curves at $\nu_N$, the difference in absorbance between the two spectra at several other values of $\nu$ are then determined, the derivatives are evaluated at the corresponding values of $\nu$ as required for eq 9, and the quantity $[G(u)/\{1-G(u)\}^2]$ is evaluated from a linear least squares fit. From $G(u)$ and eq 6, a value of $u$ is obtained from which $E_i$ is evaluated. The more detailed numerical treatments are described in ref 8.

**Second Harmonic Generation.** The second harmonic coefficients of the sample films were determined by the Maker fringe analysis.[12,13,16] These measurements were made relative to a Y-cut quartz plate ($d_{11} = 1.2 \times 10^{-9}$ esu). In this technique, a plane sample was rotated in the path of a fundamental beam of wavelength 1064 nm from a Q-switched Nd:YAG pulse laser. The second harmonic power $P_{2\omega}$ detected is given by

$$P_{2\omega} = \frac{512\pi^3}{A}t_\omega{}^4T_{2\omega}\frac{d^2p^2(\theta)}{(n_\omega{}^2 - n_{2\omega}{}^2)^2}P_\omega{}^2\sin^2\psi \quad (10)$$

where $A$ is beam area, $t_\omega$ and $T_{2\omega}$ are the transmission factors

for the incident fundamental and the second harmonic light, respectively, $n_\omega$ and $n_{2\omega}$ are the refractive indices of the incident fundamental and the second harmonic light, respectively, $d$ is the second harmonic coefficient, $p(\theta)$ is the projection factor, and $P_\omega$ is the incident fundamental laser power.

$$\psi = \frac{\pi l}{2}\frac{4}{\lambda}(n_\omega \cos\theta_\omega - n_{2\omega}\cos\theta_{2\omega}) \tag{11}$$

where $l$ is the film thickness, $\lambda$ is the wavelength of the fundamental laser beam, and

$$\sin\theta_\omega = \sin\theta/n_\omega \qquad \sin\theta_{2\omega} = \sin\theta/n_{2\omega} \tag{12}$$

from Snell's law.

Transmission factors are defined as

$$t_\omega = \frac{2\cos\theta}{n_\omega\cos\theta + \cos\theta_\omega} \tag{13}$$

for the p-polarized fundamental light,

$$t_\omega = \frac{2\cos\theta}{n_\omega\cos\theta_\omega + \cos\theta} \tag{14}$$

for the s-polarized fundamental light, and

$$T_{2\omega} = 2n_{2\omega}\cos\theta_{2\omega}\frac{(n_\omega\cos\theta + \cos\theta_\omega)(n_{2\omega}\cos\theta_\omega + n_\omega\cos\theta_{2\omega})}{(n_{2\omega}\cos\theta_{2\omega} + \cos\theta)^3} \tag{15}$$

for the p-polarized second harmonic light.

Projection factors are defined as

$$dp(\theta) = d_{33}\left[\left(\sin^2\theta_\omega + \frac{1}{3}\cos^2\theta_\omega\right)\sin\theta_{2\omega} + \frac{2}{3}\cos\theta_\omega\sin\theta_\omega\cos\theta_{2\omega}\right] \tag{16}$$

for the p-polarized fundamental and p-polarized second harmonic light, where $d_{33}$ is the SHG coefficient, and

$$dp(\theta) = 2d_{31}\sin\theta_\omega\cos\theta_\omega\cos\theta_{2\omega} \tag{17}$$

for the s-polarized fundamental and p-polarized second harmonic light, where $d_{31}$ is SHG coefficient.

Coherence length $l_c$ ($=\lambda/[4|n_\omega - n_{2\omega}|]$) is calculated using refractive indices measured at 530 and 1060 nm.

## Results and Discussion

**Polymer Structure.** Figure 1 shows WAXS results in the form of diffracted intensity versus scattering angle ($2\theta$ scan) from blend samples with various concentrations of DANS dye in (a) and DANAB dye in (b). All samples were thermally annealed at 120 °C for 2 h before X-ray measurement. The $2\theta$ scans of the sample films show the peaks of the $\beta$-crystal form at 20.8, 36.8, and 41.2°.[17] Figure 2 shows the corresponding DTA profiles of these blend samples. The DTA thermogram of the annealed blend yields three exothermic peaks at 130–140, 163 (peak I), and 174 °C (peak II). Peaks I and II are assigned as melting points of $\beta$- and $\alpha$-crystallites, respectively. The endothermic peak around 130–140 °C might be ascribed to the thermodynamic relaxation, and this peak temperature depends on the annealing temperature before the DTA measurement. The endothermic area of peak I due to the melting of the $\beta$-phase decreased with the increasing DANS dye concentration in the blend. The X-ray diffraction intensity due to the $\beta$-crystallite phase at 20.8° is also reduced by the increasing DANS concentration. These

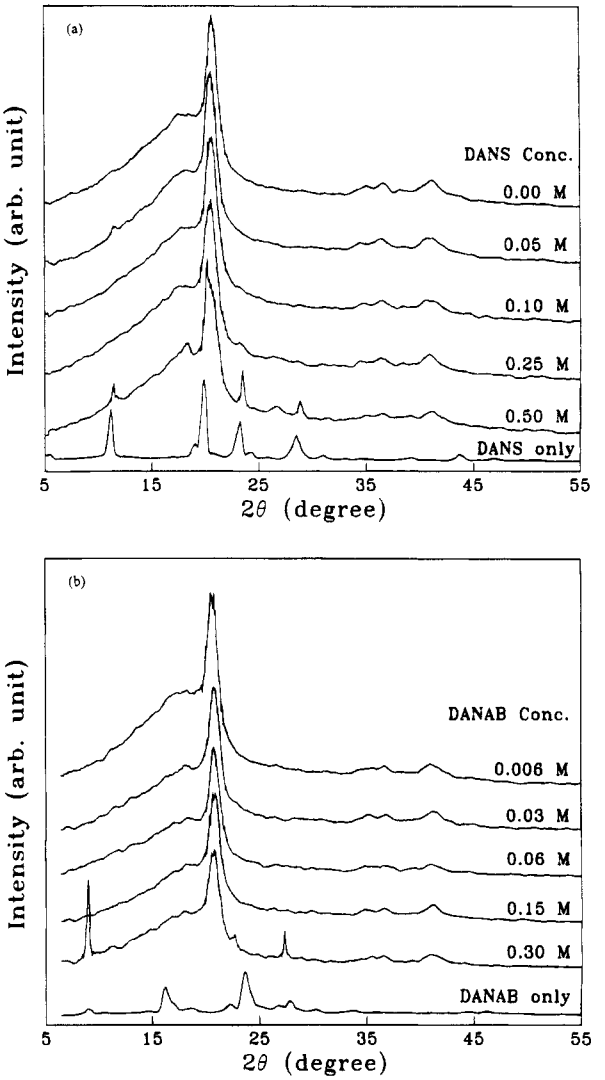


**Figure 1.** WAXS profiles for samples with various concentrations of DANS (a) and DANAB (b).

results imply that the incorporation of the larger amount of DANS molecules suppresses the crystal growth of the $\beta$-phase. However, in the case of blends dispersing the DANAB dye, the X-ray diffraction pattern and DTA endotherms do not show any significant suppression of $\beta$-crystal growth.

**NLO Dye Concentration Dependence of the Internal Electric Field.** Figure 3 is the plot of $E_i$ vs DANS concentration in the blend. $E_i$ was calculated using eq 9 with $\mu_g = 7.4$ D, $\mu_e = 24.8$ D, and $\Delta\mu = 17.4$ D for the DANS molecule.[18,19] The profile of $E_i$ decreasing with the increasing DANS concentration corresponds to the decrease of the peak area due to the melting of the $\beta$-crystallite shown in Figure 2. As described above, the crystal growth of the $\beta$-crystallite is disturbed by the incorporation of a large amount of DANS molecules, and thus $E_i$ is reduced. In the case of a DANS dye concentration of 0.1 and 0.25 M, it is difficult to calculate $E_i$ from the electrochromic shift of the DANS spectrum, because of the saturation of the absorption maximum around 435 nm due to a higher concentration of DANS molecules.

**Refractive Index.** Figure 4 shows the wavelength dependence of the refractive index (RI) for the PVDF/PMMA blend and PMMA neat films. In the case of the PMMA sample, a monotonical decrease of RI was observed with the increasing wavelength. Whereas, for the PVDF/PMMA blend, the decrease of RI was mea-

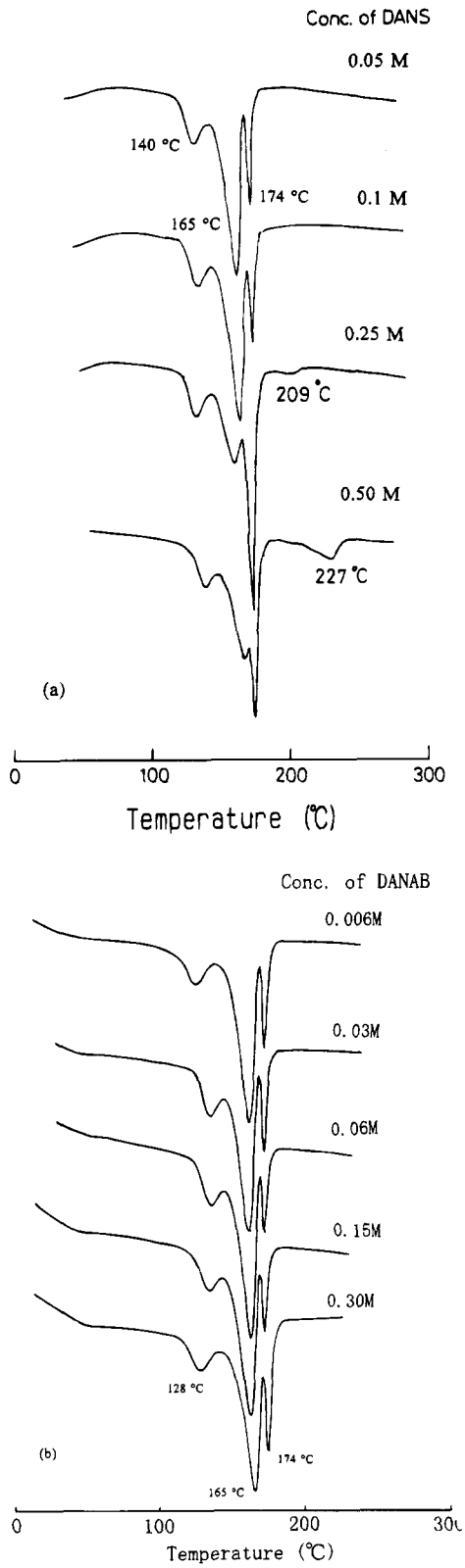


**Figure 2.** DTA profiles for samples with various concentrations of DANS (a) and DANAB (b).

sured when the wavelength of the probe light increased to 610 nm, in the wavelength region above 610 nm RI slightly increases. Table 1 shows the refractive indices measured at 470, 530, 610, 660, and 1060 nm and the coherence length calculated from the refractive indices at 530 and 1060 nm. As shown in Table 1, the coherence length is in the range 45–60 $\mu$m. For the sample with the DANS concentration above 0.03 M, the probe light in the wavelength region below 610 nm was almost completely absorbed by DANS dyes dispersed in the sample film. Therefore, no clear line between bright and dark regions in the view of an Abbe refractometer could be seen to determine the refractive index. Thus in the case of the sample with the DANS concentration above 0.03 M, the SHG coefficients $d_{33}$ and $d_{31}$ were determined using RI values for the sample with 0.02 M DANS.

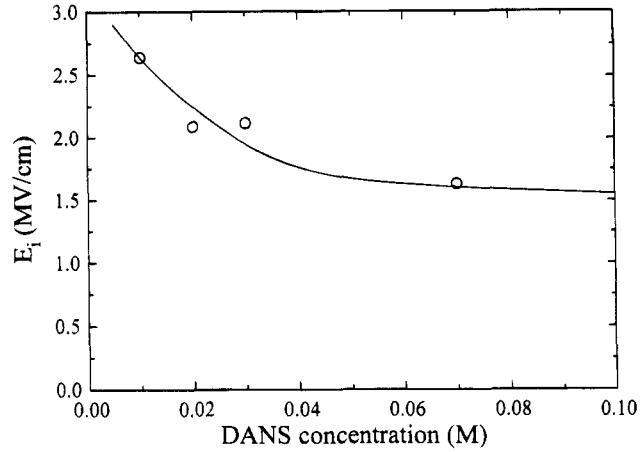


**Figure 3.** Dependence of $E_i$ on DANS content.

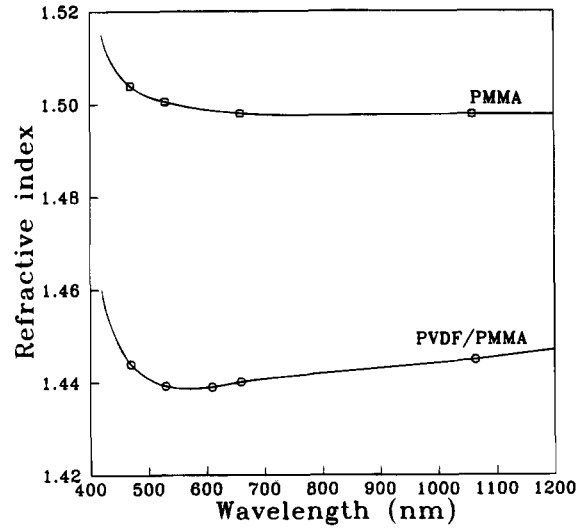


**Figure 4.** Dependence of refractive index on wavelength.

**Table 1. Refractive Index (RI) at Various Wavelengths and Coherence Lengths ($l_c$) for Samples with Various Concentrations of DANS**

| DANS (M) | RI 1060 nm | 660 nm | 610 nm | 530 nm | 470 nm | $l_c$ ($\mu$m) |
|---|---|---|---|---|---|---|
| 0.00 | 1.4448 | 1.4401 | 1.4390 | 1.4392 | 1.4439 | 47.5 |
| 0.01 | 1.4467 | 1.4421 | 1.4404 | 1.4422 | 1.4460 | 59.1 |
| 0.02 | 1.4474 | 1.4411 | 1.4390 | 1.4415 | 1.4435 | 45.1 |
| 0.03 | 1.4462 | 1.4420 | *a* | *a* | *a* | *a* |
| 0.05 | 1.4462 | 1.4424 | *a* | *a* | *a* | *a* |
| 0.07 | 1.4497 | 1.4481 | *a* | *a* | *a* | *a* |
| 0.10 | 1.4494 | 1.4465 | *a* | *a* | *a* | *a* |

[a] Impossible to measure RI due to the strong absorption by a higher concentration of DANS.

**NLO Dye Concentration Dependence of the SHG.** SHG coefficients $d_{33}$ and $d_{31}$ are shown as a function of DANS concentration in Figure 5. These values were measured 48 h after poling, at which time the initial relaxation of SHG activities seemed to be completely released. Time relaxation of the SHG coefficients $d_{33}$ and $d_{31}$ will be discussed below. The linear increase of $d_{33}$ and $d_{31}$ coefficients at a DANS concentration up to 0.03 M is mainly attributed to the linear

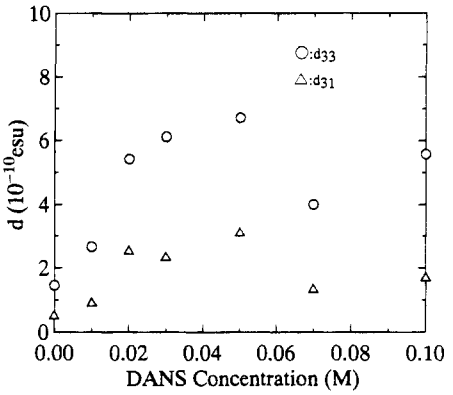


**Figure 5.** Dependence of SHG coefficients $d_{33}$ (○) and $d_{31}$ (△) on DANS content.

**Table 2. Comparison of $d_{33}$ Values Experimentally Obtained and Theoretically Calculated by Equation 18 for Samples with DANS and DANAB NLO Dyes**

| NLO dyes[a] | $d_{33}$(exp)[b] ($10^{-9}$ esu) | $d_{33}$(cal)[c] ($10^{-9}$ esu) |
|---|---|---|
| DANS | 0.61 | 1.99 |
| DANAB | 0.51 | 1.23 |

[a] NLO dye concentration is 0.03 M. [b] $d_{33}$ value experimentally obtained. [c] $d_{33}$ value theoretically calculated.

increase of SHG activity due to the increase of the DANS concentration. The SHG activities leveled out at a DANS concentration above 0.03 M, which is ascribed to the reduced $E_i$ mentioned above in addition to the reabsorption of the second harmonic light at 532 nm due to the higher DANS concentration.

In the theoretical expression of SHG, coefficient $d_{33}$[20,21] can be written as

$$d_{33} = \frac{Nf_\omega^2 f_{2\omega}\beta\mu_g E_i}{10kT} \tag{18}$$

where $N$ is the number density of noncentrosymmetric NLO guest molecules, $\beta$ is the hyperpolarizability of the NLO guest, $f_\omega$ and $f_{2\omega}$ are Lorentz–Lorenz local field factors of the form $(\epsilon + 2)/3$, and $T$ is the poling temperature. The value of $\epsilon$ has been taken as the square of the refractive index of the sample at either the fundamental or second harmonic frequency. The number of density $N$ is calculated using the film density of 1.6, and $E_i$ is the value measured for each sample. For the DANS molecule, the hyperpolarizability $\beta$ is 450 $\times$ $10^{-30}$ esu[22] and the dipole moment at the ground state $\mu_g$ is 7.4 D.[18,19] For the DANAB molecule, the product of $\mu$ and $\beta$ is 2000 $\times$ $10^{-30}$ D esu, which was obtained from that for Disperse Red 1 dye.[23] Table 2 shows the comparison of $d_{33}$ values experimentally obtained and theoretically calculated using eq 18 for the sample film with 0.03 M NLO dyes. In both cases, the experimental value of $d_{33}$ is smaller than the theoretical one. However, the prediction of the nonlinear coefficients to within 1 order of magnitude is satisfactory because of the complexity of the film morphology and consequent uncertainty in parameters required for the theoretical analysis. Namely, as described above, reabsorption of the SHG signal at 532 nm by NLO dye molecules and the reduced internal electric field at a higher concentration of NLO dye may cause the ambiguity of the comparison of the experimental value with theoretical one.

**Thermal Stability of the SHG.** Figure 6 shows the plots of $d_{33}$ and $d_{31}$ coefficients after poling as a function of the storage time at room temperature for the blend

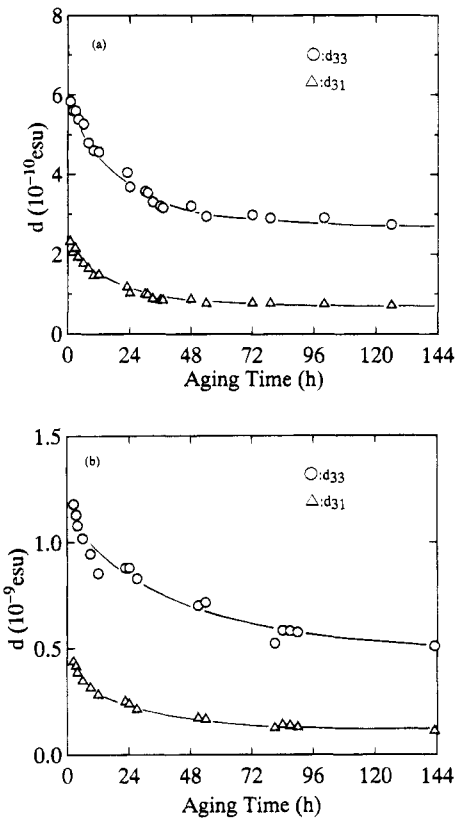


**Figure 6.** Dependence of SHG coefficients $d_{33}$ (○) and $d_{31}$ (△) on storage time for samples with 0.07 M DANS (a) and 0.03 M DANAB (b).

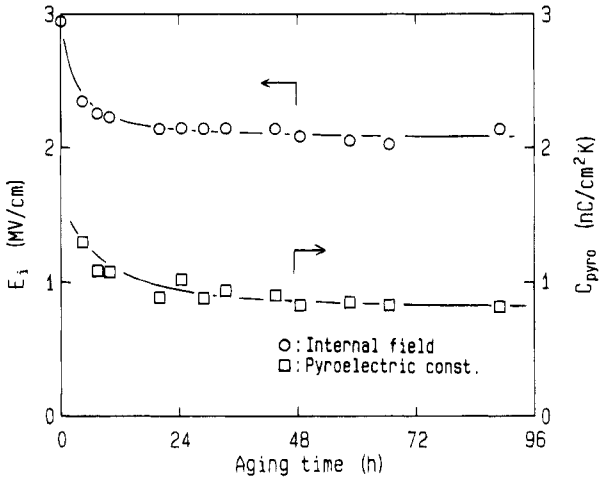


**Figure 7.** Dependence of $E_i$ (○) and $C_{pyro}$ (□) on storage time.[10]

samples including 0.07 M DANS dye (a) and 0.03 M DANAB dye (b). These aging time profiles of SHG activity can be compared with those of $E_i$ and $C_{pyro}$ shown in Figure 7 for the same blend sample which were already reported in a previous paper.[10] Initial decay profiles of SHG activities ($d_{33}$ and $d_{31}$ coefficients), $E_i$, and $C_{pyro}$ observed during the several hours immediately after poling are derived from the same nature of the blend samples. The main contribution to these decay natures may be due to the reorientation or relaxation of the aligned amorphous dipoles at room temperature, which causes the decrease of $C_{pyro}$ and $E_i$ and thus the decrease of SHG activities. The decay profile in $d_{33}$ and $d_{31}$ is more extended in time than those of $E_i$ and $C_{pyro}$. The failure to observe the proportionality between SHG activities and both $E_i$ and $C_{pyro}$ suggests that the contribution from amorphous dipoles to SHG activities is larger than that to both $E_i$

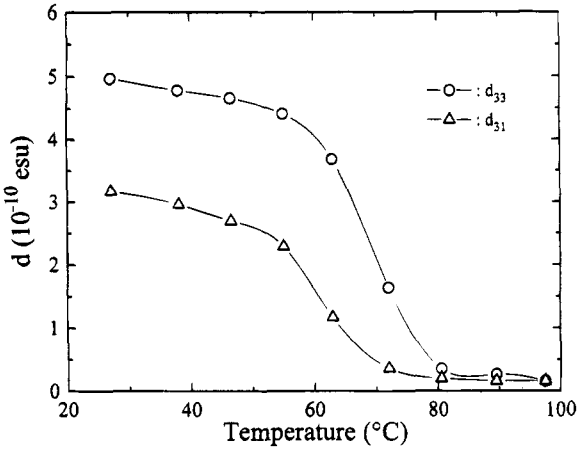


**Figure 8.** Dependence of SHG coefficients $d_{33}$ (○) and $d_{31}$ (△) on annealing temperature for samples with 0.05 M DANS.

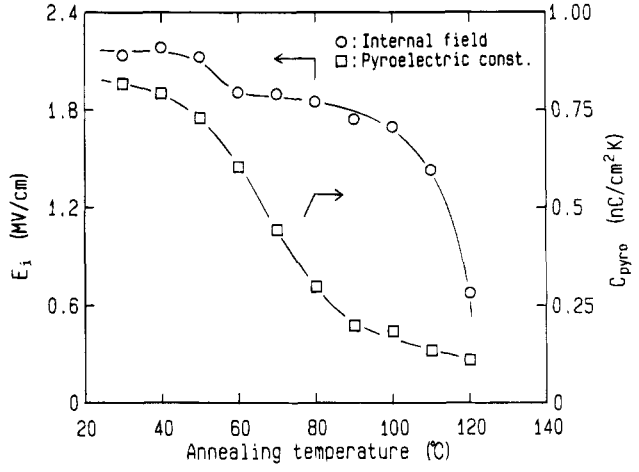


**Figure 9.** Dependence of $E_i$ (○) and $C_{pyro}$ (□) on annealing temperature.[10]

and $C_{pyro}$. Apart from the initial decay observed during the several hours immediately after poling, $d_{33}$ and $d_{31}$ coefficients remain stable in the time interval of several days during which measurements were made. The orientational stability of NLO dyes at a longer time region is ascribed to the higher stability of the internal electric field created by the aligned $\beta$-crystallite dipoles.

Figure 8 shows $d_{33}$ and $d_{31}$ coefficients of the sample with 0.05 M DANS that was poled under the same conditions as in the case of Figure 6 and then SHG activities measured at the higher fixed temperature. The large decrease of SHG activities occurs at the temperature above $T_g$ (60 °C). The profiles of $d_{33}$ and $d_{31}$ coefficients on the thermal annealing were shared by the $C_{pyro}$ profile shown in Figure 9 which was already reported in a previous paper.[10] The drastic decrease of SHG activities and $C_{pyro}$ in the temperature region above 50 °C is ascribed to the relaxation of aligned $\beta$-crystallite dipoles above $T_g$. The thermal stability of $E_i$ of the same sample, which was also reported in a previous paper,[10] is shown in Figure 9. $E_i$ shows a thermal stability extending well above $T_g$ to at least 100 °C, which was explained by the negative space charge effect injected from the electrode.[10] It is noted that the internal electric field due to space charge cannot contribute to the alignment of NLO dyes. The reorientation of aligned NLO dyes follows the relaxation of oriented crystallite dipoles by molecular motion at the temperatures above $T_g$.

## Conclusion

The SHG activities from NLO dyes dispersed in the amorphous phase of a PVDF/PMMA blend matrix were studied. NLO dyes were preferentially aligned by the internal electric field created by the oriented $\beta$-crystallite dipoles. The nature of the SHG activities loss corresponds well to the relaxation of oriented $\beta$-crystallite dipoles in the temperature region above $T_g$, which is shared by the temperature profile of pyroelectric activity.[10]

**Acknowledgment.** We gratefully acknowledge Dr. G. Thomas Davis, Polymer Division, National Institute of Standards & Technology, U.S.A., for helpful discussion and Dr. Aime S. DeReggi for numerous discussions. This work is supported in part by Grants-in-Aid for Scientific Research, No. 04650810, and for International Scientific Research, Joint Research No. 03044090, from the Ministry of Education, Science, and Culture, Japan.

## References and Notes

(1) Eich, M.; Sen, A.; Looser, H.; Bjorklund, G. C.; Swalen, J. D.; Twieg, R.; Yoon, D. Y. *J. Appl. Phys.* **1989**, *66*, 2559.
(2) Eich, M.; Reck, B.; Yoon, D. Y.; Willson, G. C.; Bjorklund, G. C. *J. Appl. Phys.* **1989**, *66*, 3241.
(3) Papers presented in: *Organic Materials for Non-linear Optics II*; Hann, R. A., Bloor, D., Eds.; The Royal Society of Chemistry: Cambridge, U.K., 1991.
(4) Jungbauer, D.; Reck, B.; Twieg, R.; Yoon, D. Y.; Willson, C. G.; Swalen, J. D. *Appl. Phys. Lett.* **1990**, *56*, 2610.
(5) Ranon, P. M.; Shi, Y.; Steier, W. H.; Xu, C.; Wu, B.; Dalton, L. R. *Appl. Phys. Lett.* **1993**, *62*, 2605.
(6) Boogers, J. A. F.; Klaase, P. Th. A.; de Vliger, J. J.; Tinnemans, A. A. *Macromolecules* **1994**, *27*, 205.
(7) Stähelin, M.; Burland, D. M.; Ebert, M.; Miller, R. D.; Smith, B. A.; Twieg, R. J.; Volksen, W.; Walsh, C. A. *Appl. Phys. Lett.* **1992**, *61*, 1626.
(8) Tsutsumi, N.; Davis, G. T.; DeReggi, A. S. *Macromolecules* **1991**, *24*, 6392.
(9) Tsutsumi, N.; Ueda, Y.; Kiyotsukuri, T. *Polymer* **1992**, *33*, 3305.
(10) Tsutsumi, N.; Ueda, Y.; Kiyotsukuri, T.; DeReggi, A. S.; Davis, G. T. *J. Appl. Phys.* **1993**, *74*, 3366.
(11) Tsutsumi, N.; Ono, T.; Kiyotsukuri, T. *Macromolecules* **1993**, *26*, 5447.
(12) Maker, P. D.; Terhune, R. W.; Nisenoff, M.; Savage, C. M. *Phys. Rev. Lett.* **1962**, *8*, 21.
(13) Jerphagnon, J.; Kurtz, S. K. *J. Appl. Phys.* **1970**, *40*, 1667.
(14) Liptay, W. In *Excited States*; Lim, E. C., Ed.; Academic Press: New York and London, 1974; Vol. I, pp 129–229.
(15) Havinga, E. E.; van Pelt, P. *Ber. Bunsen-Ges. Phys. Chem.* **1979**, *83*, 816.
(16) Prasad, P. N.; Williams, D. J. In *Introduction to Nonlinear optical Effects in Molecules & Polymers*; Prasad, P. N., Williams, D. J., Eds.; Wiley-Interscience: New York, 1991; Chapter 6.
(17) Davis, G. T.; Mckinney, J. E.; Broadhurst, M. G.; Roth, S. C. *J. Appl. Phys.* **1978**, *49*, 4998.
(18) Czekalla, J.; Wick, G. *Z. Elektrochem.* **1961**, *65*, 727.
(19) Minkin, V. I.; Osip, O. A.; Zhdanov, Y. A. *Dipole Moments in Organic Chemistry*; Plenum Press: New York and London, 1970; p 278.
(20) Singer, K. D.; Kuzyk, M. G.; Sohn, J. E. In *Nonlinear Optical and Electroactive Polymers*; Prasad, P. N., Ulrich, D. R., Eds.; Plenum Press: New York, 1988; pp 189–204.
(21) Prasad, P. N.; Williams, D. J. In *Introduction to Nonlinear optical Effects in Molecules & Polymers*; Prasad, P. N., Williams, D. J., Ed.; Wiley-Interscience: New York, 1991; Chapter 4, pp 66–73.
(22) Oudar, J. L. *J. Chem. Phys.* **1977**, *67*, 446.
(23) Amano, M. In *Advanced Non-Linear Optical Organic Materials I*; Nakanishi, H., Kobayashi, T., Nakamura, A., Umegaki, S., Eds.; CMC: Tokyo, 1991; Chapter 2, pp 125–129.

MA941245X